Food Chemistry: X 24 (2024) 101879

Contents lists available at ScienceDirect

Food Chemistry: X

journal homepage: www.sciencedirect.com/journal/food-chemistry-x

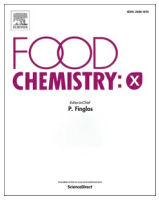

Novel sulphur-selective method for simultaneous determination of thiram and asomate based on carbon dots and its application in fruits

Lijun Wei [a,b], Mengdie Cai [b], Bixiao Zhou [b], Ping Yuan [b], Guowen Zhang [a,*], Xianglei Cheng [b,**]

[a] State Key Laboratory of Food Science and Resources, Nanchang University, Nanchang 330047, PR China
[b] Jiangxi Province Key Laboratory of Disease Prevention and Public Health, School of Public Health, Jiangxi Medical College, Nanchang University, Nanchang 330006, PR China

ARTICLE INFO

Keywords:
Thiram
Asomate
N-doped carbon dots
Sulphur-selective chemiluminescence

ABSTRACT

Thiram (THI) and asomate (ASO) are frequently detected agrochemicals in food samples due to widespread use as fungicides. However, their detection suffers from matrix interference, or the necessity of derivatization before measurement. Integrating HPLC with a post-column carbon dots (CDs)–enhanced chemiluminescence (CL) system makes it possible to simultaneously separate and selectively detect ASO and THI in fruit samples free of derivatization and deep purification. The studies on mechanisms demonstrated that CD intermediates of anionic radical were responsible for the remarkable CL enhancement of ASO or THI. The CL intensity is directly proportional to the fungicide concentration, with the ranges of linearity for ASO and THI being 5–250 μg·L^{-1} (R^2 = *0.9993*) and 4–200 μg·L^{-1} (R^2 = *0.9986*), respectively, and the corresponding limits of detection (S/N = 3) being 1.61 and 1.33 μg·L^{-1}, respectively. The developed method enables the exploration of the novelly sulphur-targeted CL application based on carbon nanomaterials.

1. Introduction

Thiram (THI) and asomate (ASO) are dimethyldithiocarbamates (DMDCs), which are a type of organic sulphur fungicides. These organic sulphur pesticides are commonly used for seed and soil treatment and in the production of food, fruits, and vegetables to control the growth of pests, weeds, and bacteria(Veiga-del-Baño et al., 2023). The extensive use of DMDC fungicides has raised concerns about their potential impact on human and animal health(He et al., 2024). Moreover, ASO functions as a fungicidal agent for DMDCs and contains arsenic. Arsenic can be converted to arsenate, leading to considerable arsenic contamination in soil and groundwater(Martinez-Garcia et al., 2022). Therefore, developing a sensitive method for detecting various types of DMDC residues in food and the environment is crucial.

GC–MS(da Silva et al., 2022) and GC–PFPD(da Silva et al., 2021) are used to detect DMDCs by measuring the CS_2 released under acidic $SnCl_2$ conditions, indirectly quantifying the total amount of DMDCs. By contrast, HPLC(López-Fernández et al., 2012; Zhou et al., 2013) and HPLC–MS(Li et al., 2019) methods are employed to identify different types of dithiocarbamates through alkaline EDTA hydrolysis and subsequent *S*-methylation derivatization, but they cannot specify the particular type of DMDC present. Other techniques like high-performance thin-layer chromatography(Fang et al., 2024), colorimetry(Li et al., 2022), fluorescence (FL)(Erdemir et al., 2023), surface enhanced Raman spectroscopy(Zhou et al., 2024), chemiluminescence (CL)(Asghar et al., 2022), and electrochemistry(Geng et al., 2024), have also been utilized for THI determination. The common feature of these analytical methods is the measurement of total DMDCs or the detection of THI. Despite being DMDC fungicides, THI and ASO considerably differ in food safety limits and health hazards. Hence, these challenges have urged to developing new methods for both simultaneous separation and selective detection of THI and ASO is crucial.

CL has emerged as a crucial spectral analysis technique(Cai et al., 2023; Galligan et al., 2024) owing to its various advantages, such as ease of instrumentation, minimal background signal, high sensitivity, and broad linear range. The continual development of carbon dots (CDs) have garnered widespread attention from researchers (Guo et al., 2024; Huang et al., 2024; Lu et al., 2023) owing to their favorable attributes, including good water solubility, exceptional luminescent properties, tunable emission wavelengths, superior photostability, cost-

* Corresponding author at: State Key Laboratory of Food Science and Resources, Nanchang University, 235 Nanjing East Road, Nanchang city, Jiangxi province 330047, PR China.
** Corresponding author at: School of Public Health, Nanchang University, 461 Bayi Road, Nanchang 330006, PR China.
E-mail addresses: weilj@ncu.edu.cn (L. Wei), gwzhang@ncu.edu.cn (G. Zhang), chengxl@ncu.edu.cn (X. Cheng).

https://doi.org/10.1016/j.fochx.2024.101879
Received 21 July 2024; Received in revised form 2 October 2024; Accepted 3 October 2024
Available online 5 October 2024

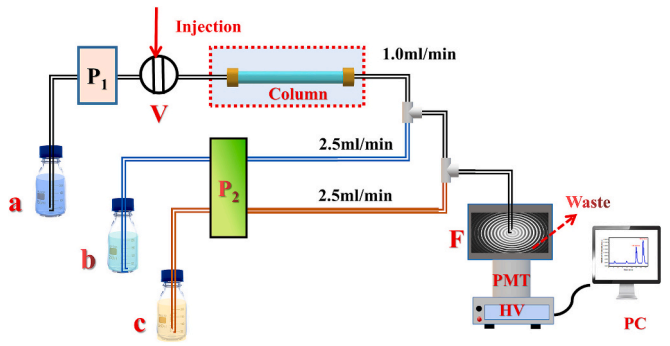

Fig. 1. Schematic diagram of the HPLC–CL method for separating and quantifying ASO and THI. (a) mobile phase, MeOH (48 %, v/v%); (b) 1000-fold diluted N-CDs; (c) 0.5 mM Ce(IV) solution containing 0.025 M sulphuric acid and 0.05 M hydrochloric acid; P_1, HPLC pump; P_2, peristaltic pump; V, injection valve; F, flow cell; PMT, photomultiplier tube; HV, negative high-voltage supply (800 V); PC, personal computer.

effectiveness, ease of synthesis, biocompatibility, and environmental friendliness. In recent years, CD-enhanced CL systems have been effectively utilized in food analysis(Dezhakam et al., 2024; Wei et al., 2024; Yi et al., 2024).

Despite these advancements, the complexity of sample matrices and the limited selectivity of CL reactions have posed challenges, impeding the broad application of CL technology. The HPLC–CL method, which effectively combines the high selectivity of the HPLC separation method with the high sensitivity of CL detection(Huertas-Pérez et al., 2016), has proven instrumental in overcoming issues related to complex sample matrix interference and is increasingly gaining traction in food safety. Ce (IV) has been identified as a stable oxidant in CL systems and can be utilized to establish CL systems with reagents such as $Ru(bpy)_3^{2+}$(Ikeda et al., 2014), MCLA(Li, Zeng, et al., 2018) and rhodamine 6G (Barbatsi & Economou, 2023) in HPLC–CL methods. These CL systems have been successfully applied in food analysis.

While CDs show promise as CL materials, there is a notable absence of reports on the application of CD-enhanced CL systems coupled with HPLC detection methods in practical sample detection. Further research in this direction holds the potential to address existing limitations and advance the utilization of CL technology in various analytical applications.

Herein, we observed that acidic cerium(IV) (Ce(IV)) in combination with ASO or THI can produce weak CL, which can be considerably enhanced by a sulphur-targeted N-doped carbon dots (N-CDs) created through an efficient microwave-assisted pyrolysis method. We also explored the CL mechanisms by employing FL, electron paramagnetic resonance spectroscopy, and CL spectra. After optimizing HPLC and CL parameters, a novel HPLC–CL method was developed and successfully employed to detect ASO and THI in fruits.

2. Materials and methods

2.1. Chemicals

Ultrapure water (18.2 MΩ) was prepared by a Direct-Q5 UV ultrapure water machine (Merck Millipore, USA). HPLC-grade methanol and acetonitrile were purchased from Merck (Germany).

THI (99.9 %) and 5,5-dimethyl-1-pyrroline-N-oxide (DMPO) were procured from Beijing InnoChem Science & Technology Co. Ltd. (Beijing, China). ASO (analytical standard), potassium bromide (spectroscopically pure), anhydrous citric acid (CA), L-serine (L-Ser), cerium(IV) sulfate, 2,2,6,6-tetramethyl-4-piperidone (TEMP), anhydrous sodium sulfate, and sodium hydroxide were all purchased from Aladdin Scientific Corporation (Shanghai, China). Hydrochloric acid was purchased from Xilong Scientific Co. Ltd. (Shantou, China). Quinine sulfate was acquired from Hefei Bomei Biotechnology Co. Ltd. (Hefei, China). The chemical reagents used were analytically pure and were not further purified.

Cerium(IV) sulfate (4.04 g) was dissolved in 100 mL boiling 5.0 M H_2SO_4. After cooling, water was added to bring the final volume to 100 mL, resulting in a 0.10 M Ce(IV) solution in 5.0 M H_2SO_4. A precisely weighed 10.0 mg standard sample was dissolved in 50 mL methanol to create standard stock solutions containing 200 mg·L^{-1} ASO and THI. All stock solutions were stored at 4 °C. The standard stock solutions were diluted with mobile phase to create mixed working standards containing 4–250 μg·L^{-1} of the two substances to be detected. The N-CD working solution was obtained by directly diluting the N-CD stock solution with ultrapure water.

2.2. Apparatus

The morphology of N-CDs was characterized by transmission electron microscopy (TEM) and high-resolution TEM (HRTEM) with a JEM-2100 microscope (JEOL, Japan) operating at an acceleration voltage of 200 kV. X-ray photoelectron spectroscopy (XPS) data were acquired to investigate the elemental composition and functional groups on the N-CDs using an ESCA Lab 250Xi X-ray photoelectron spectrometer (Thermo Scientific, USA). The functional groups of N-CDs were characterized using a Fourier Transform Infrared (FT-IR) spectrometer (Thermo Scientific, USA). Additionally, the FL and CL properties of the N-CDs were measured using an F-280 FL spectrophotometer (Tianjin Gangdong Scientific Co. Ltd., China). UV–vis absorption spectra were recorded with a UV-1900 spectrophotometer (Beijing Puxi General Instruments Co., Ltd., China). Finally, electron spin resonance spectra were obtained using an EPR200M electron spin resonance spectrometer (CIQTEK Co. Ltd., China).

2.3. Preparation of N-CDs

A one-pot microwave-assisted pyrolysis method was used to efficiently synthesize N-CDs, utilizing equal amounts of CA and L-Ser as precursor materials. CA and L-Ser (0.50 g each) were placed in a 30-mL PTFE crucible, and 2.5 mL ultrapure water was added to dissolve the solid. The crucible was then subjected to pyrolysis in a microwave oven at 650 W for 7 min, forming a brownish-black colloidal solid upon cooling to 25 °C. The solid was dissolved in 30 mL ultrapure water and then filtered through a 0.22-μm water-based membrane to eliminate insoluble substances, yielding a dark brown solution. This solution was purified by dialysis (MWCO, 100 Da) for 12 h to remove free low molecular weight substances. After dilution with ultrapure water to a final volume of 50.00 mL, the solution was stored at 4 °C.

2.4. HPLC–CL procedure

The HPLC–CL method is diagrammed in Fig. 1. The LC separation section includes a Waters 515 pump (Milford, MA, USA), a Rheodyne 7725i manual injection valve (Cotati, CA, USA), and a Zorbax SB-C18 column (250 × 4.6 mm, 5 μm) (Agilent Technologies, Waldbronn, Germany). The post-column CL detector comprises a peristaltic pump (BT100-1F, Baoding Longer Precision Pump Co. Ltd., China) for delivering aqueous N-CD and acidic Ce(IV) solutions at 2.5 mL/min. The N-CD solution is mixed with the column effluent and then combined with the acidic Ce(IV) solution in a homemade quartz flow cell (2 mm i. d.) to induce rapid CL. PTFE tubes (0.5 mm i. d.) connect all components within the flow system. The CL signal is captured by a photomultiplier tube (PMT) positioned directly beneath the flow cell set at 800 V and recorded by a computer equipped with a data acquisition interface. The relative CL intensity, ΔI, is calculated as $I_s - I_0$, where I_s and I_0 denote the maximum and baseline CL intensities of the sample solution, respectively. This value is used for the quantitative analysis of ASO and THI.

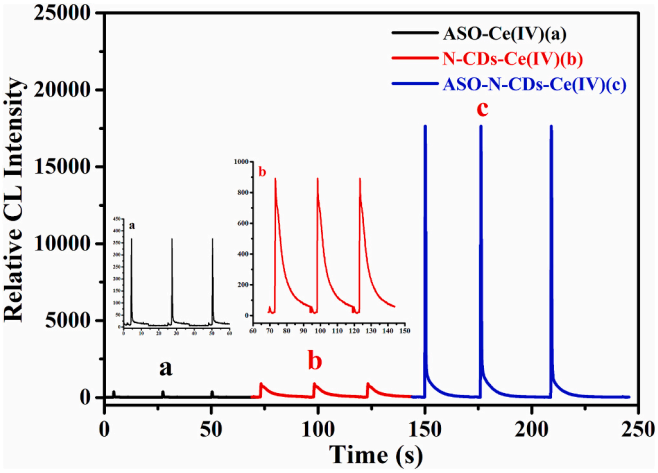

Fig. 2. CL kinetics. Conditions: Ce(IV), 1.0 mM in 0.05 M H_2SO_4 and 0.05 M HCl; N-CDs, dilution ratio was 1:2000; ASO: 100 μg·L − 1; PMT: 600 V.

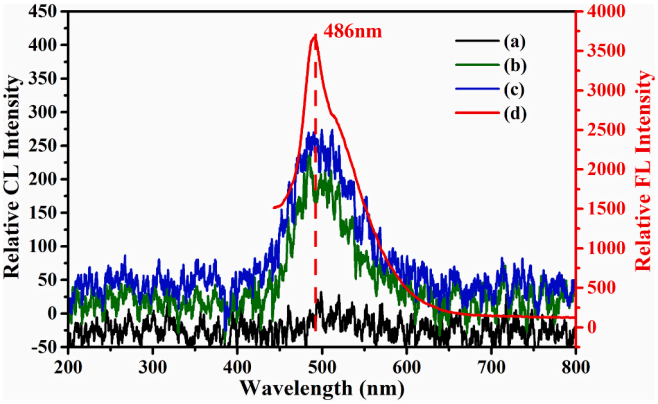

Fig. 3. The CL spectra of the (a) N-CDs-Ce(IV) system (black line), (b) N-CDs-ASO-Ce(IV) system (green line), (c) N-CDs-THI-Ce(IV) system (blue line), and (d) PL of N-CD system after reaction at 420 nm (red line). (For interpretation of the references to colour in this figure legend, the reader is referred to the web version of this article.)

2.5. Sample preparation

Tomatoes, peaches, grapes, apples, and pears were purchased from a local agricultural market in Nanchang, China. After washing the fruits and vegetables with tap water to remove surface dirt, they were dried using filter paper and diced into small pieces using a QSJ-B03H2 household meat grinder (Bear, China). The samples were evenly dispersed using an XHF-D high-speed homogenizer (Ningbo Scientz Biotechnology Co. Ltd., China). The homogenized samples weighing exactly 5.00 (±0.01) g were added to 50-mL PTFE centrifuge tubes. Subsequently, the pH of each sample was adjusted to 7.0 using a 2.0 M NaOH solution, followed by the addition of 30.0 mL toluene. The centrifuge tubes were then placed in an LC Portex MT multitube vortex mixer (Lichen, China) and vigorously shaken for 30 min. The samples were centrifuged at 10,000 r·min^{-1} for 5 min, and the upper organic phase was collected. This extraction process was repeated twice. The collected organic phases were combined and then dehydrated with anhydrous sodium sulfate. The solvent was removed by vacuum rotary evaporation at 50 °C. Subsequently, 5.0 mL of mobile phase was added, and the resultant solution was sonicated for 5 min to dissolve any residue. After filtration with a 0.22-μm organic filter membrane, the samples were stored at −20 °C in the dark. Samples were prepared in triplicate and measured three times.

2.6. Statistical analysis

All experiments were carried out in three replicates, and results were displayed as mean ± SD. Data were analyzed using a one-way analysis of variance (ANOVA), followed by Duncan's test. $p < 0.05$ was considered significant.

3. Results and discussion

3.1. CL kinetics

The kinetic curve of the CL reaction vividly demonstrates the formation and energy release of CL emitters. Upon injecting 100 μL of acidic Ce(IV) into the ASO solution (Fig. 2a), a faint CL was detected, persisting for less than 2 s, indicating a rapid reaction. In contrast, injecting 100 μL of acidic Ce(IV) into the N-CD solution resulted in a CL signal of greater intensity and longer duration (Fig. 2b). When 100 μL of Ce(IV) was injected into the mixed solution of ASO and N-CDs (Fig. 2c), a very strong CL signal was produced, nearly 60 times higher than that of the ASO-Ce(IV) CL system. The observed trend of the CL intensity transitioning from strong to weak suggests at least two reactions and the presence of ASO may catalyze the CL reaction of the N-CDs-Ce(IV) CL system and enhance its CL intensity. Consequently, N-CDs play a crucial role in enhancing the emission of this CL system.

3.2. Putative CL mechanisms

We initially conducted CL spectra measurements to understand how N-CDs boost the CL of acidic Ce(IV)-ASO and -THI. With the excitation light slit turned off, the reaction solution was continuously mixed using a peristaltic pump to generate CL, and the CL signal was captured using a FL spectrophotometer. As shown in Fig. 3a, the combination of N-CDs and acidic Ce(IV) resulted in CL emission, with a peak at 486 nm. The CL intensity significantly increased when introducing ASO (green line in Fig. 3b) and THI (blue line in Fig. 3c) into the CL system. At the same time, the emission peak wavelength remained constant at 486 nm. This suggests that ASO and THI can enhance the CL intensity of the N-CDs-Ce(IV) system.

Under an excitation wavelength of 420 nm, we recorded the photoluminescence (PL) spectra of post-reaction N-CDs (oxidated N-CDs, Ox-N-CDs) (Fig. 3d). The results showed that the maximum emission wavelength of the FL spectrum of Ox-N-CDs aligns with the maximum emission wavelength in the CL spectrum, both at 486 nm. There was a notable red shift between the maximum emission wavelength of post-reaction N-CDs and pre-reaction N-CDs. This suggests that the N-CDs after the reaction are likely to be CL emitters, and the presence of ASO and THI enhances the yield of CL emitters.

Prior studies of CL systems(Teng et al., 2023) using CDs have usually shown associations with reactive oxygen species (ROS). In this experiment, the solution was treated with oxygen or nitrogen to remove oxygen, but the CL intensity of the system remained unaffected. Additionally, ROS capture probes TEMP and DMPO were used, but no significant signals were detected, indicating that the generation of CL in the system is not dependent on ROS.

Prior researches(Asghar et al., 2019; Asghar et al., 2022) have indicated that BrO_3^- and Ag(III) can trigger a reaction with THI, leading to the generation of excited state SO_2*, and CL, which can be enhanced by chemiluminescence resonance energy transfer (CRET) with quinine. Furthermore, quinine has been found to enhance the CL of Ce(IV) and THI(Waseem et al., 2010). The authors suggest that Ce(IV) and THI can produce Ce(III)*. In order to ensure whether CL generating from CRET between SO_2* or Ce(III)* and Ox-N-CDs, the reaction product of Ce(IV) with N-CDs was dialyzed and mixed with Ce(IV) and THI/ASO for further reaction. Unfortunately, no significant CL enhancement was noted. Methyl dimethylcarbamate was tested instead of ASO or THI in the present CL system and no enhancement was observed, which

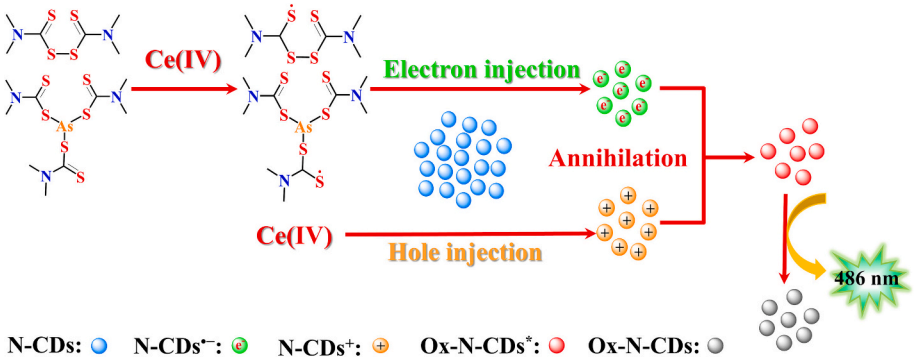

Fig. 4. Putative mechanism of N-CDs-Ce(IV) CL systems enhanced by THI and ASO.

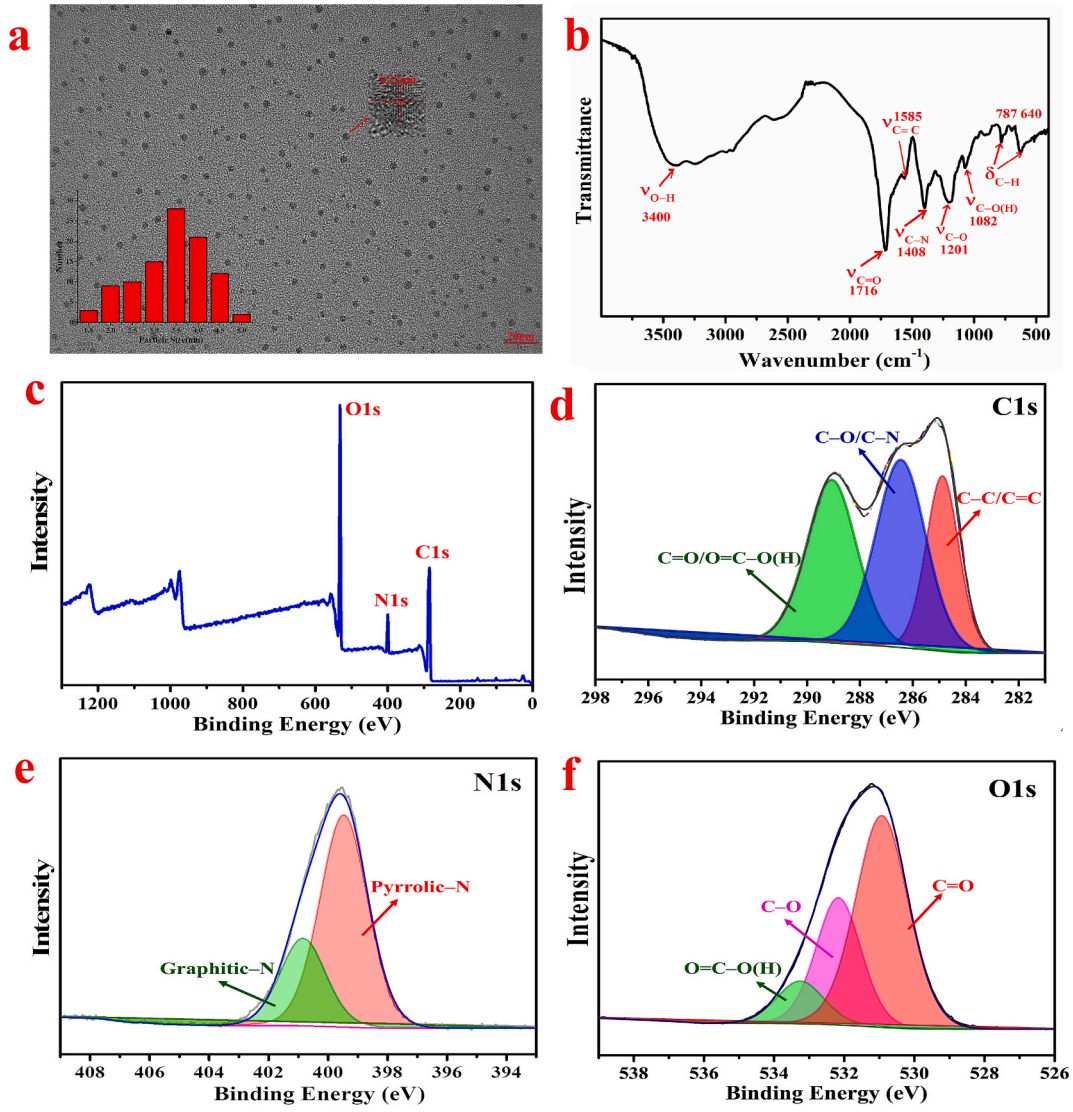

Fig. 5. (a) TEM and (b) FT-IR spectra; (c) wide scan XPS spectrum; (d) high-resolution XPS spectra of C1s, (e) N1s, and (f) O1s of N-CDs.

suggested that sulphur atom was rather vital in the present CL reaction.

Based on the experimental findings, the mechanisms of CL can be inferred as follows: Ce(IV) could directly oxidize N-CDs with the formation of excited state Ox-N-CDs*(Lin et al., 2012; Wei et al., 2024). As the Ox-N-CDs* return to their ground state, they emit light at 486 nm. This part of CL is responsible for the background emission. The intermediate products formed by the oxidation of THI and ASO by Ce(IV) can inject electrons into N-CDs, resulting in the formation of N-CDs$^{\bullet-}$(Xue et al., 2011). Simultaneously, N-CDs can undergo redox reactions with Ce(IV), forming N-CDs$^{\bullet+}$. The annihilation between N-CDs$^{\bullet+}$ and N-CDs$^{\bullet-}$ gives rise to the production of excited state oxidation of N-CDs, Ox-N-CDs*, accompanied by the generation of 486 nm CL (Li, Lai, et al., 2018). A schematic representation of this reaction mechanism is depicted in Fig. 4.

Table 1
Previously reported methods for the determination of ASO and THI (μg·kg^{-1}).

Method	Derivatizing agent	LOD		Sample	Ref.
		THI	ASO		
HPLC–DAD	Alkaline EDTA/CH_3I	9.75	–	Apple, tomato Cucumber, corn	(Zhou et al., 2013)
HPLC–SERS	None	240	–	Orange, Longan	(Wang et al., 2015)
UPLC–MS/MS	None	4.40	–	Papaya, banana, pineapple, guava	(Zhao et al., 2021)
HPLC–UV	None	–	100	Apple and soil	(Huang et al., 2016)
GC–MS	$SnCl_2$/HCl	15.80	–	Yerba mate	(da Silva et al., 2022)
GC–MS	$SnCl_2$/HCl	58.50	–	Soybean leaf, pod, seed, oil, and soil	(Chawla et al., 2019)
GC–PFPD GC–ITD–MS	$SnCl_2$/HCl	15.83	–	Soybean	(da Silva et al., 2021)
HPLC–CL	None	1.33	1.61	Apples, grapes, pears, peaches, tomatoes	This method

3.3. Chromatography optimization

Li's group (Wang et al., 2021) utilized a Zorbax Plus C18 chromatography column (150 mm × 4.6 mm, 5 μm) with water-acetonitrile as the mobile phase for analyzing THI in wheat flour and flour modifiers. Subsequently, the Zorbax SB-C18 (250 mm × 4.6 mm, 5 μm) column was selected to separate THI and ASO. The results showed that the two compounds could be fully separated using methanol or acetonitrile solution as the mobile phase. A 48 % methanol (MeOH: H_2O, *v*/v) solution was ultimately chosen for the mobile phase, due to methanol's inhibitory effect on the present CL system, with a flow rate of 1.0 mL·min^{-1}. The compounds were successfully separated within 16 min at 25 °C.

3.4. N-CD synthesis conditions and CL

Our preliminary studies suggest that N-CDs play a crucial role in the CL system. CDs synthesized from CA and L-Ser have been shown to significantly enhance the CL emissions of Ce(IV)-ASO and THI. Interestingly, N-CDs synthesized through microwave pyrolysis were more effective in enhancing the CL than those prepared by solvothermal and solid-state pyrolysis methods. As a result, the microwave-assisted pyrolysis method was chosen for N-CD preparation. Moreover, both the precursor mass ratio and the duration of microwave heating impacted the sensitization efficiency.

To determine the optimal mass ratio of the two precursors, N-CDs were synthesized using a constant total precursor weight of 1.0 g, with varying mass ratios of CA to L-Ser (2:1, 1.5:1, 1:1, 1:1.5, 1:2, 1:2.5, and 1:3). The results, illustrated in Fig. S1a, revealed that the CL intensity of the N-CDs-Ce(IV)-ASO (THI) system significantly increased when the mass ratio changed from 2:1 to 1:1. However, a mass ratio less than 1:1 weakened the CL signal, likely due to the evaporation of water during microwave heating, leaving only molten CA and L-Ser in the crucible.

CA has a melting point of 153 °C–159 °C versus 240 °C for L-Ser. Therefore, CA is a precursor for synthesizing N-CDs and acts as a cosolvent. An increase in the amount of L-Ser elevates the reaction

Table 2
Intraday and interday average recoveries (%) and RSD (%) for thiram and asomate in different food matrices ($n = 5$).

Matrix	Spiked level	Thiram						Asomate					
		Intraday (μg·kg^{-1})			Interday (μg·kg^{-1})			Intraday (μg·kg^{-1})			Interday (μg·kg^{-1})		
		Concentration	Recovery	RSD	Concentration	Recovery	RSD	Concentration	Recovery	RSD	Concentration	Recovery	RSD
Apple	0	0	–	–	0	–	–	0	–	–	0	–	–
	20	15.07 ± 1.05	75.35	6.98	14.05 ± 1.10	70.25	7.83	17.27 ± 0.85	86.37	4.92	15.06 ± 1.10	75.31	7.31
	50	40.16 ± 1.55	80.32	3.85	37.64 ± 1.76	75.28	4.67	47.62 ± 2.79	95.23	5.86	45.62 ± 2.08	91.24	6.56
	100	93.31 ± 3.67	93.31	3.93	85.65 ± 3.43	85.65	3.96	108.10 ± 3.53	108.10	3.27	104.16 ± 5.18	104.16	4.97
Tomato	0	0	–	–	0	–	–	0	–	–	0	–	–
	20	14.48 ± 0.81	72.41	5.59	14.29 ± 0.81	71.43	5.67	15.09 ± 0.87	75.45	5.77	14.20 ± 0.91	70.98	6.41
	50	41.74 ± 1.96	83.48	4.69	39.12 ± 1.95	78.24	4.99	52.73 ± 2.33	105.46	4.43	50.56 ± 2.46	101.12	4.87
	100	88.12 ± 2.63	88.12	2.98	86.56 ± 4.55	86.56	5.26	107.32 ± 3.72	107.32	3.47	104.29 ± 5.14	104.29	4.93
Pear	0	0	–	–	0	–	–	0	–	–	0	–	–
	20	14.73 ± 0.84	73.67	5.70	14.53 ± 1.05	72.67	7.24	17.10 ± 1.05	85.70	6.14	16.83 ± 1.14	84.14	6.77
	50	40.23 ± 1.65	80.46	4.13	38.24 ± 1.96	76.48	5.13	48.62 ± 1.84	97.23	3.78	46.83 ± 2.36	93.65	5.04
	100	89.36 ± 3.55	89.36	3.97	82.36 ± 4.09	82.36	4.97	107.67 ± 3.43	107.67	3.19	102.54 ± 1.45	102.54	4.34

Matrix	Spiked level[a]	Thiram						Asomate					
		Intraday (μg·kg^{-1})			Interday (μg·kg^{-1})			Intraday (μg·kg^{-1})			Interday (μg·kg^{-1})		
		Concentration	Recovery	RSD	Concentration	Recovery	RSD	Concentration	Recovery	RSD	Concentration	Recovery	RSD
Grape	0	0	–	–	0	–	–	0	–	–	0	–	–
	20	14.86 ± 0.59	74.32	6.57	14.68 ± 0.76	73.41	6.18	16.86 ± 1.14	84.32	6.75	17.42 ± 1.12	87.12	6.43
	50	41.07 ± 1.53	82.13	5.73	40.59 ± 2.19	81.17	5.40	46.74 ± 1.97	93.47	4.21	45.64 ± 2.27	91.27	4.97
	100	90.16 ± 2.31	90.16	3.56	87.90 ± 3.86	87.90	4.39	104.23 ± 3.68	104.23	3.53	103.47 ± 4.40	103.47	4.26
Peach	0	0	–	–	0	–	–	0	–	–	0	–	–
	20	15.48 ± 0.79	77.24	5.10	14.85 ± 0.90	74.23	6.06	17.88 ± 1.03	89.41	5.74	17.53 ± 0.96	87.63	5.48
	50	40.83 ± 1.70	81.65	4.16	40.37 ± 1.97	80.73	4.87	50.10 ± 1.56	100.23	4.11	48.43 ± 2.59	96.86	5.35
	100	91.14 ± 3.52	91.14	3.86	85.86 ± 3.80	85.86	4.43	106.89 ± 3.59	106.89	3.36	105.53 ± 4.95	105.53	4.69

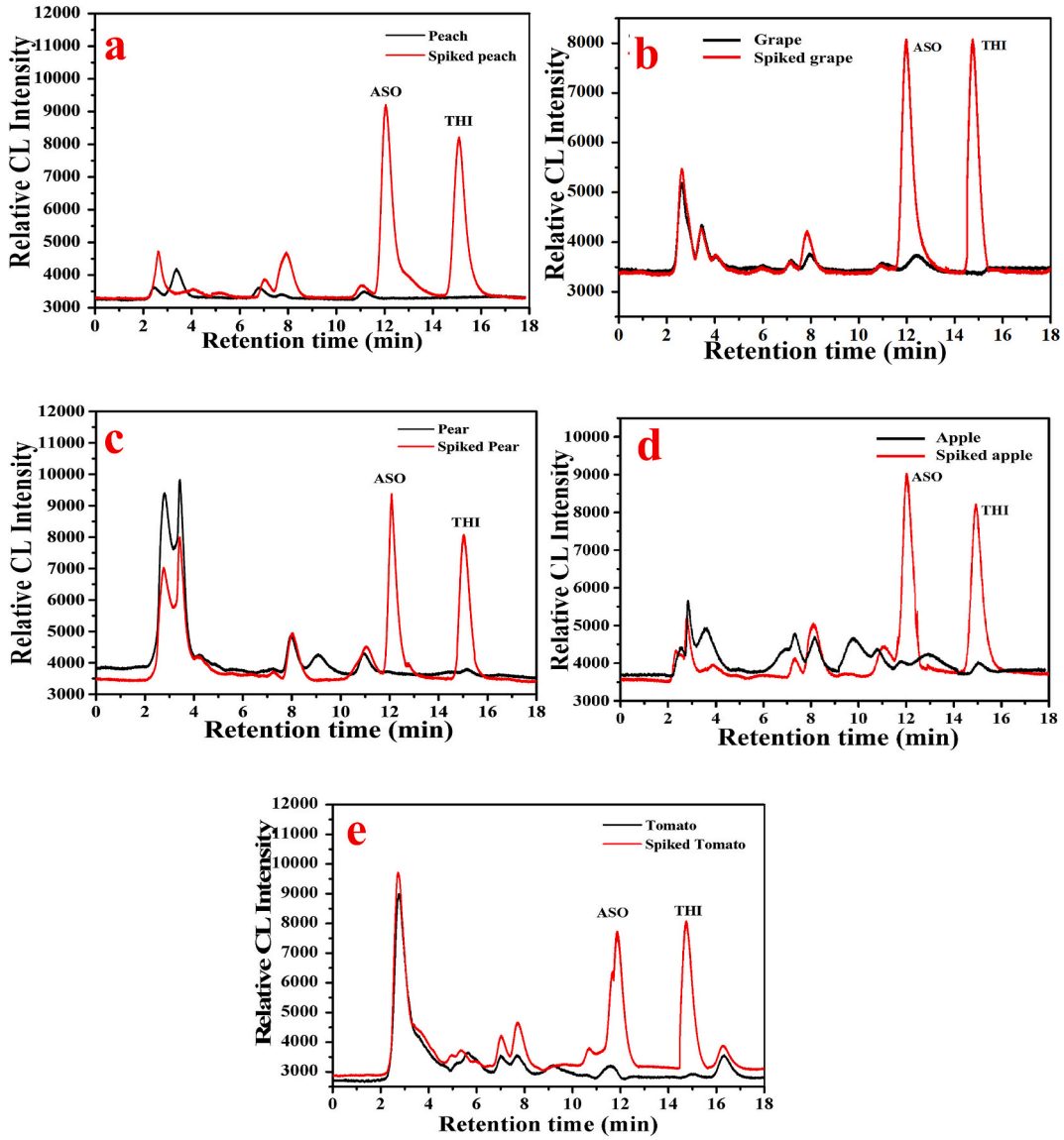

Fig. 6. Chromatography curve of (a) pear and spiked samples (b) grape and spiked samples (c) apple and spiked samples (d) tomato blank and spiked samples (e) peach and spiked samples.

center's temperature, intensifying the carbonization process and damaging the functional groups of N-CDs involved in the CL reaction, leading to a decrease in CL. Therefore, the optimal mass ratio for the synthesis of N-CDs is 1:1. At this ratio, the equilibrium between COOH and OH in CA and L-Ser is achieved, facilitating the generation of CL.

Subsequent investigation focused on the impact of microwave synthesis time on the CL of ASO and THI, as demonstrated in Fig. S1b. The findings indicated that the CL emission intensities of ASO and THI peaked at a synthesis time of 7 min, suggesting that the 4–7 min period was critical for forming CDs. Beyond this timeframe, with increased carbonization, CDs precipitated due to diminished water solubility, thereby reducing the signal. As a result, the optimal synthesis conditions for producing N-CDs for subsequent experiments were determined to be a 1:1 mass ratio of CA to L-Ser and a synthesis time of 7 min.

3.5. Characterization of N-CDs

3.5.1. Optical properties of N-CDs

The visual appearance of the N-CD solution is depicted in the Fig. S2a inset. N-CDs appear almost colorless in natural light, but under 365 nm ultraviolet radiation, they emit bright blue light due to edge effects and quantum confinement. As shown in Fig. S2a, the PL spectrum of N-CDs exhibits wavelength dependence. When excited with wavelengths ranging from 330 nm to 460 nm, the maximum excitation wavelength of N-CDs shows a noticeable red shift. This shift may be attributed to the presence of various functional groups, reaction sites, and surface defects in N-CDs, similar to the FL properties of CDs reported in the literature (Nelson et al., 2024). Additionally, the UV–Vis spectra of N-CDs are shown in Fig. S2b. N-CDs exhibit two broad UV absorption bands near 210 nm and 380 nm, corresponding to the $\pi \rightarrow \pi^*$ transition of the C═C conjugated band and the $n \rightarrow \pi^*$ transitions of the C═O and C═N bands, respectively. The maximum emission and excitation wavelength of carbon dots were 483 nm and 380 nm, respectively.

3.5.2. Morphology and surface structural characteristics of N-CDs

The microstructure, size distribution, and crystallographic characteristics of the synthesized N-CDs are illustrated in Fig. 5a. The N-CDs are nearly spherical particles with uniform size and good dispersion, ranging from 2.0 nm to 5.0 nm with an average particle size of 3.56 ± 0.42 nm. The HRTEM image (Fig. 5a inset) reveals a distinct lattice stripe structure with a lattice spacing of 0.22 nm, consistent with the in-plane lattice spacing of graphene (100)(Ferjani et al., 2024), indicating

the formation of graphene-like structures during the microwave-assisted pyrolysis process.

The surface functional group structure of N-CDs was analyzed using FT-IR (Fig. 5b), which revealed several absorption peaks ranging from 4000 to 500 cm^{-1}. The broad peak at 3400 cm^{-1} and the prominent peak at 1728 cm^{-1} correspond to the stretching vibration peaks of O—H and C═O, respectively, indicating the presence of numerous carboxyl groups on N-CDs. Additionally, stretching vibration absorption peaks at C═C (1585 cm^{-1}), C—N (1408 cm^{-1}), C—O (1201 cm^{-1}), and C–O(H) (1082 cm^{-1}) were also identified(Li et al., 2020). Furthermore, the N—H and O—H bending vibration absorption peaks at 787 cm^{-1} and 640 cm^{-1}, respectively, may be present on the surface of N-CDs(Nelson et al., 2024).

The composition, content, and functional groups of N-CDs were analyzed using XPS. The XPS spectrum of N-CDs indicates that they are mainly composed of C, N, and O (Fig. 5c). The binding energies of C1s, O1s, and N1s were 286 eV, 533 eV, and 401 eV, respectively, confirming the successful nitrogen doping during synthesis. The atomic percentages of C, N, and O are 61.23 %, 8.34 %, and 30.43 %, respectively. The high-resolution XPS spectrum of C1s (Fig. 5d) revealed three peaks at binding energies of 284.8 eV, 286.3 eV, and 288.8 eV, corresponding to C–C/C=C, C–O/C–N, and C=O/O–C=C, respectively. The high-resolution XPS spectrum of N1s (Fig. 5e) showed two peaks at binding energies of 399.2 eV and 401.3 eV, corresponding to sp^3 C–N/C–N–C (pyrrolic-N) and sp^2 C═N (pyridinic-N), respectively. The prevalence of pyrrolic-N over pyridinic-N suggests that carboxylic acids and amino groups primarily formed amides during the microwave process. The high-resolution XPS spectrum of O1s (Fig. 5f) exhibited three peaks at binding energies of 530.7 eV, 532.0 eV, and 533.1 eV, respectively, corresponding to C═O, O–C=O, and C—O (H). The FT-IR and XPS spectra indicated that the surface of N-CDs was rich in hydrophilic groups such as carboxylic acids, amides, and hydroxyl groups, contributing to their good water solubility.

3.6. CL optimization

In this study, the sensitivity of the method depends on the concentration of N-CDs, the concentration of the oxidant Ce(IV), the acidic environment, and the flow rate. Univariate methods were utilized to optimize these CL parameters to achieve high-sensitivity detection of ASO and THI.

3.6.1. Effect of N-CD concentration

The concentration of N-CDs, an essential CL reagent, significantly impacted sensitivity. To determine the optimal concentration, an N-CD stock solution was diluted in series (500-, 1000-, 2000-, 3000-, 4000-, 5000-, and 6000-fold). Utilizing the proposed HPLC–CL method, we tested the effect of these dilutions on the CL signal when determining the concentrations of two analytes with a mass concentration of 200 $\mu g \cdot L^{-1}$. As shown in Fig. S3a, the results indicated that the CL intensity of ASO peaked at a 1000-fold dilution and then declined sharply with further dilution. Conversely, the CL intensity of THI gradually increased with increasing dilution of N-CDs. Beyond a 4000-fold dilution ratio, the CL intensity decreased gradually due to insufficient N-CD concentration. Given these findings, we opted for a dilution ratio of 1000-fold for N-CDs as optimal for subsequent experiments.

3.6.2. Effect of Ce(IV) concentration

Ce(IV) is the sole oxidant in the CL system, and its concentration significantly influences the CL intensity. To enhance detection sensitivity, we studied the impact of Ce(IV) concentration on CL within the range of 0.2 to 2.0 mM (Fig. S3b). The CL peaked at 0.5 mM and then gradually declined as the concentration increased. The Ce(IV) concentration had a similar effect on the CL of THI and ASO. Consequently, we selected 0.5 mM Ce(IV) as the optimum for subsequent experiments.

3.6.3. Effect of acidic media

Acidic conditions can enhance the stability of the Ce(IV) solution and preserve its oxidizing properties; however, the CL intensity may vary with differences in the acidic medium. Preliminary experiments showed that an acid with a hydrogen ion concentration of 0.05 M favored CL generation. Therefore, hydrochloric acid, acetic acid, nitric acid, methanesulfonic acid, perchloric acid, and 0.025 M sulphuric acid were selected as the acid media, all maintained at 0.05 M, to study their impact on the CL intensity of ASO and THI at the same concentration (Fig. S3c). The findings revealed that the two analytes generated the strongest CL in a 0.05 M hydrochloric acid medium. Consequently, hydrochloric acid was chosen as the medium.

Furthermore, the strength of the solution affected the luminescence intensity. We investigated the impact of hydrochloric acid concentration on the luminescence of ASO and THI within the 0 to 0.10 M range. As shown in Fig. S3d, within the concentration range of 0.02 to 0.05 M, the CL intensity increased with increasing hydrochloric acid concentration, peaking at 0.05 M for both analytes. However, when the concentration exceeded 0.05 M, the baseline noise increased, and the CL of the two analytes sharply decreased. Therefore, we selected 0.05 M hydrochloric acid for subsequent experiments.

3.6.4. Effect of flow rate

The peristaltic pump transports CL reaction reagents merging with eluents after they've passed through the column. Therefore, the flow rate is a significant parameter influencing CL intensity. The flow rate of the peristaltic pump was optimized over a range of 1.0 to 5.0 $mL \cdot min^{-1}$ (Fig. S3e). Upon varying the flow rate from 1.0 to 2.0 $mL \cdot min^{-1}$, the THI CL intensity peaked at 1.5 $mL \cdot min^{-1}$ and did not change significantly between that point and 2.0 $mL \cdot min^{-1}$. This is consistent with the results of the CL kinetic curve which revealed a rapid reaction, with CL increasing with the flow rate. Additionally, methanol in the mobile phase has a certain inhibitory effect on CL, and methanol dilution in the mobile phase enhances CL with an increasing flow rate. However, as the flow rate increases, the concentration of THI is diluted by the CL reagent, resulting in a gradual decrease in CL.

The behavior of ASO differed from that of THI. As the flow rate increased from 1.0 to 2.50 $mL \cdot min^{-1}$, the CL of ASO increased, possibly due to methanol-mediated inhibition of the ASO-N-CDs-Ce(IV) CL system in the mobile phase, requiring a higher flow rate. However, when the flow rate exceeded 2.5 $mL \cdot min^{-1}$, the CL decreased. To achieve highly sensitive detection of both substances, the flow rate of the peristaltic pump was set to 2.5 $mL \cdot min^{-1}$.

3.7. Analytical performance

The method was validated under optimal conditions per regulations of EU 2002/657/EC Decision. The standard chromatograms of THI and ASO analytes at 200 $\mu g \cdot L^{-1}$ are shown in Fig. S4a. The retention times for ASO and THI were 11.87 and 14.91 min, respectively, with their separation and detection achieved within 16 min. A standard curve was plotted using eight different concentrations of mixed standard solution (4.0 $\mu g \cdot L^{-1}$ to 250 $\mu g \cdot L^{-1}$), as shown in Fig. S4b. Table S1 illustrates a strong linear relationship for THI and ASO within the concentration range of 4.0 $\mu g \cdot L^{-1}$ to 200 $\mu g \cdot L^{-1}$ and 5.0 $\mu g \cdot L^{-1}$ to 250 $\mu g \cdot L^{-1}$, respectively. The linear correlation coefficients (R^2) were determined to be 0.9986 and 0.9993, respectively. The limits of detection (LOD, S/N = 3) for THI and ASO were 1.33 $\mu g \cdot L^{-1}$ and 1.61 $\mu g \cdot L^{-1}$, respectively. The relative standard deviation (RSD) of the retention times for both analytes was below 0.55 %, while the RSD of peak heights was below 1.54 %.

A comparison of the proposed new HPLC–CL method with existing methods for THI and ASO in foods, as summarized in Table 1, showed that this method has significantly higher sensitivity than HPLC–DAD (Zhou et al., 2013) and HPLC–UV(Huang et al., 2016). Furthermore, compared with other mass spectrometry methods, such as UPLC–MS/MS

(Zhao et al., 2021) and GC–MS(da Silva et al., 2022), it demonstrated lower LOD and higher sensitivity.

3.8. Application of real samples

To assess the practical applicability of the proposed method, we a conducted a study on five fruit samples (apple, grape, pear, peach, tomato). Our findings, presented in Table 2, indicate that the intraday and interday recoveries and RSDs of THI in food substrates ranged from 70.23 % to 93.31 % and 3.19 % to 7.31 %, respectively. Similarly, the incorporation recoveries and RSD of ASO were 70.98 % to 108.11 % and 2.27 % to 5.32 %, respectively. These results validate the excellent spiked recovery and detection accuracy of the method. Additionally, our analysis revealed that the two DMDC compounds are robustly stable in 48 % methanol. Our chromatographic separation of the fruit samples, shown in Fig. 6, demonstrated that interfering substances in the matrix did not significantly impact the detection of ASO and THI. The HPLC–CL detection method, validated through practical sample analysis, effectively addressed the issues of interference and insufficient sensitivity encountered in the application of HPLC–UV/DAD and GC–MS methods.

4. Conclusion

In this study, a novel approach for the simultaneous detection of THI and ASO using the HPLC-CL technique is put forward based on their selectively catalytic effect on the CL reaction between Ce(IV) and CDs. The remarkable CL enhancement is achieved through the formation of N-CDs$^{\bullet-}$ stemming from reduction effect of THI and ASO. Subsequently, the proposed HPLC–CL method provides a stable baseline, minimal background noise, and high sensitivity. Furthermore, unlike existing methods, it eliminates laborious steps such as derivatization and further purification via solid phase extraction while achieving efficient separation of ASO and THI in just 16 min. This study offers a fresh perspective on the CL mechanism of carbon nanomaterials and the application of HPLC and CL coupling technology.

CRediT authorship contribution statement

Lijun Wei: Writing – original draft, Methodology, Funding acquisition. **Mengdie Cai:** Methodology. **Bixiao Zhou:** Validation. **Ping Yuan:** Data curation. **Guowen Zhang:** Writing – review & editing, Supervision. **Xianglei Cheng:** Writing – review & editing, Funding acquisition, Conceptualization.

Declaration of competing interest

We declare that we have no financial and personal relationships with other people or organizations that can inappropriately influence our work, there is no professional or other personal interest of any nature or kind in any product, service and/or company that could be construed as influencing the position presented in, or the review of, the manuscript entitled, "*Novel sulphur-selective method for simultaneous determination of thiram and asomate based on carbon dots and its application in fruits*".

Data availability

Data will be made available on request.

Acknowledgements

The authors would like to thank for the financial supports from the National Natural Science Foundation of China (Nos. 82373631, 82173574 and 81960600) and Training Program of Innovation and Entrepreneurship for Undergraduates of Jiangxi Province (No. YC2023-B047).

Appendix A. Supplementary data

Supplementary data to this article can be found online at https://doi.org/10.1016/j.fochx.2024.101879.

References

Asghar, M., Yaqoob, M., Munawar, N., & Nabi, A. (2022). Determination of thiram residues in fresh water using flow injection diperiodatonickelate(IV)-quinine chemiluminescence detection. *Luminescence, 37*(12), 2041–2049. https://doi.org/10.1002/bio.4389

Asghar, M., Yaqoob, M., & Nabi, A. (2019). Potassium bromate-quinine chemiluminescence detection of thiram in water samples using flow injection analysis. *Journal of Analytical Chemistry, 74*(4), 323–329. https://doi.org/10.1134/s1061934819040038

Barbatsi, M., & Economou, A. (2023). Programmable low-pressure chromatographic sub-90 s assay of parabens in cosmetics with post-column chemiluminescence detection. *Separations, 10*(6). https://doi.org/10.3390/separations10060350

Cai, M., Gan, W., Ding, Z., Cai, H., Wei, L., & Cheng, X. (2023). Studies on reaction mechanisms and distinct chemiluminescence from cyanoimino neonicotinoids triggered by peroxymonosulfate in advanced oxidation processes. *Chinese Chemical Letters, 34*(3), Article 107554. https://doi.org/10.1016/j.cclet.2022.05.068

Chawla, S., Patel, H. K., Kalasariya, R. L., & Shah, P. G. (2019). Validation and analysis of thiram, a dithiocarbamate, as CS_2 from soybean (*Glycine max*) samples on GC-MS. *International journal of Environmental Science and Technology, 16*(11), 6991–6998. https://doi.org/10.1007/s13762-018-2069-0

Dezhakam, E., Tavakkol, M., Kafili, T., Nozohouri, E., Naseri, A., Khalilzadeh, B., & Rahbarghazi, R. (2024). Electrochemical and optical (bio)sensors for analysis of antibiotic residuals. *Food Chemistry, 439*, Article 138145. https://doi.org/10.1016/j.foodchem.2023.138145

Erdemir, S., Oguz, M., & Malkondu, S. (2023). Cu^{2+}-assisted sensing of fungicide thiram in food, soil, and plant samples and the ratiometric detection of Hg^{2+} in living cells by a low cytotoxic and red emissive fluorescent sensor. *Journal of Hazardous Materials, 452*, Article 131278. https://doi.org/10.1016/j.jhazmat.2023.131278

Fang, G., Hasi, W., Lin, X., & Han, S. (2024). Automated identification of pesticide mixtures via machine learning analysis of TLC-SERS spectra. *Journal of Hazardous Materials, 474*, Article 134814. https://doi.org/10.1016/j.jhazmat.2024.134814

Ferjani, H., Abdalla, S., Oyewo, O. A., & Onwudiwe, D. C. (2024). Facile synthesis of carbon dots by the hydrothermal carbonization of avocado peels and evaluation of the photocatalytic property. *Inorganic Chemistry Communications, 160*, Article 111866. https://doi.org/10.1016/j.inoche.2023.111866

Galligan, J. J., Baeumner, A. J., & Duerkop, A. (2024). Recent advances and trends in optical devices and sensors for hydrogen peroxide detection. *TrAC, Trends in Analytical Chemistry, 180*, Article 117948. https://doi.org/10.1016/j.trac.2024.117948

Geng, L., Sun, X., Wang, L., Liu, F., Hu, S., Zhao, S., & Ye, F. (2024). Analyte-induced laccase-mimicking activity inhibition and conductivity enhancement of electroactive nanozymes for ratiometric electrochemical detection of thiram. *Journal of Hazardous Materials, 463*, Article 132936. https://doi.org/10.1016/j.jhazmat.2023.132936

Guo, B., Chen, F., Liu, G., Li, W., Li, W., Zhuang, J., Zhang, X., Wang, L., Lei, B., Hu, C., & Liu, Y. (2024). Effects and mechanisms of proanthocyanidins-derived carbon dots on alleviating salt stress in rice by muti-omics analysis. *Food Chem. X, 22*, Article 101422. https://doi.org/10.1016/j.fochx.2024.101422

He, G., Xie, R., Hou, X., Yu, X., Qiu, S., Qin, S., Wang, F., & Chen, X. (2024). Safety risk of using asomate to reduce acid in *Citrus* production. *Journal of Food Composition and Analysis, 134*, Article 106537. https://doi.org/10.1016/j.jfca.2024.106537

Huang, P., Liu, X., Wang, L., Peng, Y., & Luo, M. (2016). Determination of asomate residues in apple and soil. *Chinese Journal of Analysis Laboratory, 35*(1), 86–89.

Huang, X., Zhao, W., Sun, W., Li, Z., Zhang, N., Shi, J., Zhang, Y., Zhang, X., Shen, T., & Zou, X. (2024). A paper-based ratiometric fluorescent sensor for NH_3 detection in gaseous phase: Real-time monitoring of chilled chicken freshness. *Food Chem. X, 21*, Article 101054. https://doi.org/10.1016/j.fochx.2023.101054

Huertas-Pérez, J. F., Moreno-González, D., Airado-Rodríguez, D., Lara, F. J., & García-Campaña, A. M. (2016). Advances in the application of chemiluminescence detection in liquid chromatography. *TrAC, Trends in Analytical Chemistry, 75*, 35–48. https://doi.org/10.1016/j.trac.2015.07.004

Ikeda, R., Ichiyama, K., Tabuchi, N., Wada, M., Kuroda, N., & Nakashima, K. (2014). Determination of folates by HPLC-chemiluminescence using a ruthenium (II)-cerium (IV) system, and its application to pharmaceutical preparations and supplements. *Luminescence, 29*(7), 824–830. https://doi.org/10.1002/bio.2627

Li, A. X., Li, H. X., Ma, Y., Wang, T. H., Liu, X. M., Wang, C. G., … Lu, G. Y. (2022). Bioinspired laccase-mimicking catalyst for on-site monitoring of thiram in paper-based colorimetric platform. *Biosensors & Bioelectronics, 207*, Article 114199. https://doi.org/10.1016/j.bios.2022.114199

Li, J., Dong, C., Yang, Q., An, W. J., Zheng, Z. T., & Jiao, B. N. (2019). Simultaneous determination of ethylenebisdithiocarbamate (EBDC) and propylenebisdithiocarbamate (PBDC) fungicides in vegetables, fruits, and mushrooms by ultra-high-performance liquid chromatography tandem mass spectrometry. *Food Analytical Methods, 12*(9), 2045–2055. https://doi.org/10.1007/s12161-019-01538-z

Li, J., Zeng, W. S., Lai, X. J., Wang, X., Xu, X., Cai, H. P., … Cheng, X. L. (2018). Selective and sensitive determination of tetracyclines by HPLC with chemiluminescence detection based on a cerium(IV)-methoxylated cypridina luciferin analogue system.

Journal of Separation Science, 41(22), 4115–4121. https://doi.org/10.1002/jssc.201800683

Li, L., Lai, X., Xu, X., Li, J., Yuan, P., Feng, J., Wei, L., & Cheng, X. (2018). Determination of bromate via the chemiluminescence generated in the sulfite and carbon quantum dot system. *Microchimica Acta, 185*(2), 163. https://doi.org/10.1007/s00604-017-2653-x

Li, Y., Yang, Y., Jiang, Y., & Han, S. (2020). Detection of tannic acid exploiting carbon dots enhanced hydrogen peroxide/potassium ferricyanide chemiluminescence. *Microchemical Journal, 157*, Article 105113. https://doi.org/10.1016/j.microc.2020.105113

Lin, Z., Xue, W., Chen, H., & Lin, J.-M. (2012). Classical oxidant induced chemiluminescence of fluorescent carbon dots. *Chemical Communications, 48*(7), 1051–1053. https://doi.org/10.1039/c1cc15290d

López-Fernández, O., Rial-Otero, R., González-Barreiro, C., & Simal-Gándara, J. (2012). Surveillance of fungicidal dithiocarbamate residues in fruits and vegetables. *Food Chemistry, 134*(1), 366–374. https://doi.org/10.1016/j.foodchem.2012.02.178

Lu, B., Chen, X., Ouyang, X., Li, Z., Yang, X., Khan, Z., Duan, S., & Shen, H. (2023). The roles of novel chitooligosaccharide-peanut oligopeptide carbon dots in improving the flavor quality of Chinese cabbage. *Food Chem. X, 20*, Article 100963. https://doi.org/10.1016/j.fochx.2023.100963

Martinez-Garcia, M. M., Pichardo-Molina, J. L., Arzate-Plata, N., & Alvarado-Gil, J. J. (2022). Concave gold nanoparticles on aluminum as surface enhanced Raman spectroscopy substrate for detection of thiram. *Nanomaterials and Nanotechnology, 12*. https://doi.org/10.1177/18479804221082778

Nelson, D. J., Vasimalai, N., John, S. A., & Sethuraman, M. G. (2024). Turn-off fluorometric determination of bilirubin using facile synthesized nitrogen-doped carbon dots as a fluorescent probe. *Journal of Fluorescence*. https://doi.org/10.1007/s10895-023-03572-x

da Silva, R. C., dos Santos, I. D., Neu, J. P., Wouters, R. D., Fontana, M. E. Z., Balbinot, P. D. R., … Pizzutti, I. R. (2022). Commercial yerba mate (Ilex paraguariensis) produced in South America: Determination of dithiocarbamate residues by gas chromatography-mass spectrometry. *Food Chemistry, 394*, Article 133513. https://doi.org/10.1016/j.foodchem.2022.133513

da Silva, R. C., Wickert, C., Pizzutti, I. R., & de Kok, A. (2021). Clean-up strategy for dithiocarbamate fungicide determination in soybean by GC-ITD-MS and GC-PFPD: Method development and validation. *Journal of Agricultural and Food Chemistry, 69*(38), 11485–11493. https://doi.org/10.1021/acs.jafc.1c01870

Teng, X., Qi, L., Liu, T., Li, L., & Lu, C. (2023). Nanomaterial-based chemiluminescence systems for tracing of reactive oxygen species in biosensors. *TrAC, Trends in Analytical Chemistry, 162*. https://doi.org/10.1016/j.trac.2023.117020

Veiga-del-Baño, J. M., Martínez-López, S., Pérez-Lucas, G., Cuenca-Martínez, J. J., & Andreo-Martínez, P. (2023). Trends in dithiocarbamates food research: A bibliometric vision. *Chemosphere, 313*, Article 137342. https://doi.org/10.1016/j.chemosphere.2022.137342

Wang, W., Xu, M. M., Guo, Q. H., Yuan, Y. X., Gu, R. N., & Yao, J. L. (2015). Rapid separation and on-line detection by coupling high performance liquid chromatography with surface-enhanced Raman spectroscopy. *RSC Advances, 5*(59), 47640–47646. https://doi.org/10.1039/c5ra05562h

Wang, X., Zhou, S., Li, X., & Zhang, Q. (2021). Determination of thiram in wheat flour and flour improvers by high performance liquid chromatography-diode array detection. *Chinese Journal of Chromatography, 39*(6), 652–658. https://doi.org/10.3724/sp.j.1123.2020.07024

Waseem, A., Yaqoob, M., & Nabi, A. (2010). Determination of thiram in natural waters using flow-injection with cerium(IV)-quinine chemiluminescence system. *Luminescence, 25*(1), 71–75. https://doi.org/10.1002/bio.1147

Wei, L., Gan, W., Cai, M., Cai, H., Zhang, G., & Cheng, X. (2024). Development of a novel HPLC-CDCL method utilizing nitrogen-doped carbon dots for sensitive and selective detection of dithiocarbamate pesticides in tea. *Food Chemistry, 458*, Article 140237. https://doi.org/10.1016/j.foodchem.2024.140237

Xue, W., Lin, Z., Chen, H., Lu, C., & Lin, J.-M. (2011). Enhancement of ultraweak chemiluminescence from reaction of hydrogen peroxide and bisulfite by water-soluble carbon nanodots. *Journal of Physical Chemistry C, 115*(44), 21707–21714. https://doi.org/10.1021/jp207554t

Yi, Z., Xiao, S., Kang, X., Long, F., & Zhu, A. (2024). Bifunctional MOF-encapsulated cobalt-doped carbon dots nanozyme-powered chemiluminescence/fluorescence dual-mode detection of aflatoxin B1. *ACS Appl. Mat. Interfaces, 16*(13), 16494–16504. https://doi.org/10.1021/acsami.4c00560

Zhao, J., Pu, J., Wu, X., Chen, B., He, Y., Zhang, Y., & Han, B. (2021). Evaluation of the matrix effect of pH value and sugar content on the analysis of pesticides in tropical fruits by UPLC-MS/MS. *Microchemical Journal, 168*, Article 106375. https://doi.org/10.1016/j.microc.2021.106375

Zhou, H., Qiu, J., Zhang, Y., Liang, Y., Han, L., & Zhang, Y. (2024). Self-assembled C-ag hybrid nanoparticle on nanoporous GaN enabled ultra-high enhancement factor SERS sensor for sensitive thiram detection. *Journal of Hazardous Materials, 469*, Article 133868. https://doi.org/10.1016/j.jhazmat.2024.133868

Zhou, L., Xu, J., Luan, L., Ma, J., Gong, Y., Qin, D., & Pan, C. (2013). Optimization validation of a method based on derivatization with methylating agent followed by HPLC-DAD for determining dithiocarbamates residues. *Acta Chromatographica, 25*(4), 613–625. https://doi.org/10.1556/AChrom.25.2013.4.2